Submitted to ApJ

X-winds in Action

Mike J. Cai[1], Hsien Shang[1], Hsiao-Hsuan Lin[2], Frank H. Shu[3]

[1]*Academia Sinica, Institute of Astronomy and Astrophysics, Taiwan*
[2]*Department of Physics, University of Southern California*
[3]*Department of Physics, University of California, San Diego*

mike@asiaa.sinica.edu.tw

ABSTRACT

The interaction of accretion disks with the magnetospheres of young stars can produce X-winds and funnel flows. With the assumption of axial symmetry and steady state flow, the problem can be formulated in terms of quantities that are conserved along streamlines, such as the Bernoulli integral (BI), plus a partial differential equation (PDE), called the Grad-Shafranov equation (GSE), that governs the distribution of streamlines in the meridional plane. The GSE plus BI yields a PDE of mixed type, elliptic before critical surfaces where the flow speed equals certain characteristic wave speeds are crossed and hyperbolic afterward. The computational difficulties are exacerbated by the locations of the critical surfaces not being known in advance. To overcome these obstacles, we consider a variational principle by which the GSE can be attacked by extremizing an action integral, with all other conserved quantities of the problem explicitly included as part of the overall formulation. To simplify actual applications we adopt the cold limit of a negligibly small ratio of the sound speed to the speed of Keplerian rotation in the disk where the X-wind is launched. We also ignore the obstructing effects of any magnetic fields that might thread a disk approximated to be infinitesimally thin. We then introduce trial functions with adjustable coefficients to minimize the variations that give the GSE. We tabulate the resulting coefficients so that other workers can have analytic forms to reconstruct X-wind solutions for various astronomical, cosmochemical, and meteoritical applications.

Subject headings: stars: pre-main-sequence; winds; ISM: accretion disks; jets and outflows; MHD

1. Introduction

Accretion, disks, and jets are ubiquitous in astrophysics (see, e.g., Blandford & Rees 1992). A consensus has been reached that an extra needed ingredient to obtain outflow from inflow is the presence of strong magnetic fields that thread a disk conventionally assumed to be rotating at Keplerian speeds about a central gravitating object, taken in this paper to be a newly born star. Differences come in ascribing the origin of the magnetic fields in the disk itself or in the central star (Königl & Pudritz 2000, Shu et al. 2000).

Disk winds have been extensively studied, both analytically via the assumptions of self-similarity in 2-D space for axisymmetric, time-independent flows (e.g., Blandford & Payne 1982; Contopoulos & Lovelace 1994) or by taking advantage of arbitrary variations of the gas pressure (e.g., Tsinganos & Trussoni 1991) or by studying the asymptotic properties of the collimation (Heyvaerts & Norman 1997); and numerically by finite-element methods attacking the axisymmetric, time-independent, Grad-Shafranov equation (e.g., in the relativistic regime by Camenzind 1987) or by finite-difference treatments of the time-dependent equations of ideal MHD in 2- and 3-D (e.g., Uchida & Shibata 1986, Pudritz et al. 2006). For a review of these types of calculations, see Ferreira (2004).

The most highly developed semi-analytic theory for the second viewpoint is called X-wind theory, in which fast jets arising in young stellar objects (YSOs) owe their existence to the interaction of the accretion disk with the magnetosphere of the central star. The interaction of accretion disks with strongly magnetized central stars has also been studied numerically (e.g., Goodson, Bohm, & Winglee 1999; Long et al. 2005, Ustyugova et al. 2006). Although both funnel flows and X-like winds have been found, they have yet to appear simultaneously in numerical simulations, probably because the numerical calculations have not yet proceeded to steady state where the condition of disk-locking applies (Shu et al. 1994). Pure X-wind theory assumes for simplicity that the disk itself is unmagnetized, in fact, all that is needed for the theory to work is for open field lines to be concentrated in a narrow annulus near the inner edge of an accretion disk.

Recently, Bacciotti et al. (2002) and Coffey et al. (2004) identified jet rotation in four T Tau systems, DG Tau, TH 28, RW Aur, and LkHα 321, of an amount too large to be compatible with X-winds, but consistent with launching from disks at radii of 0.5-2 AU. Later, Cabrit et al. (2006) showed from mm-wave radio measurements that the disk rotation in RW Aur is actually in the opposite sense to that deduced for the jet from optical lines. Moreover, Pety et al. (2006) find that HH 30, which is observed nearly edge-on and therefore should have had the clearest signature for jet rotation, showed no evidence for outflow rotation at mm wavelengths, a conclusion reinforced by optical and ultraviolet observations of the HH 30 jet by Coffey et al. (2007). While the positive results remain for the three other systems,

the case of HH 30, where longitudinal velocities occur in the direction transverse to the line of sight, suggests that the slight line asymmetries in the other cases may be more associated with unequal jumps in the velocity of shocked, high-speed jets, than to the rotation of collimated outflows.

In contrast, no one has proposed any explanation other than X-winds for the correlated inflow-outflow signatures seen in SU Aur by Giampapa et al. (1993) and Johns & Basri (1995). Apart from SZ 68 (Johns-Krull & Hatzes 1997), we are unaware of any other T Tau star that shows a tilted-dipole magnetic-field geometry, and it could be that the dipole component is small on the surface of most T Tau stars (Johns-Krull 2007). Fortunately, Mohanty & Shu (2007) show that while funnel flows are sensitive to the detailed assumptions made concerning multi-pole structure on the surfaces of the central stars, the properties of the X-wind depend mostly only on the amount of trapped flux in the X-region (see also the observational evidence relating to this point collected by Johns-Krull & Gafford 2002).

Recent calculations show that YSOs are unlikely to lose enough magnetic flux in the process of gravitational collapse to make the level of magnetization ignorable in the resultant circumstellar accretion disks (Galli et al. 2006; Shu et al. 2006, 2007). Indeed, the disks are sufficiently magnetized in many cases that, in quasi-steady state, they rotate at sub-Keplerian rates until the the inner disk-edge is reached. Thus, there are open questions of how much of the trapped flux near the inner edge is to be attributed to the central star versus the disk, and how such disks reacquire near-Keplerian rates of rotation at their inner edges. We ignore these complications in the present study of the X-wind phenomenon, but we note that the methods introduced here are easily modified to attack the more complex problem when the accretion disk interacting with a stellar magnetosphere is itself strongly magnetized.

The original X-wind model supposed the outflow to occur from the equator of a magnetized star spun to breakup by a presence of an accretion disk that abutted its surface (Shu et al. 1988). Later, in order to accommodate the slow rotators, such as the classical T Tauri stars which are only rotating at one tenth of breakup (Vogel & Kuhi 1981, Bouvier et al. 1991, Edwards et al. 1993), Shu et al. (1994a) generalized the X-wind picture to include the case of relatively low accretion when the magnetosphere of the star would truncate the accretion disk at an inner edge before the disk reached the stellar surface (typically a circle of radius 0.2 on the scale of Fig.1, where the disk's inner edge is taken to be at $\varpi = 1$). In a quasi-steady-state where most of the mass of the central star is built up by disk accretion, the magnetic coupling between the star and the disk regulates the star to corotate at the Keplerian frequency at the truncation radius. For a protostar with magnetic dipole moment μ_*, mass M_*, mass accretion rate $\dot{M}_D$, Ostriker & Shu (1995) estimate this radius to be

$$R_X = \Phi_{\rm dx}^{-4/7} \left(\frac{\mu_*^4}{G M_* \dot{M}_D^2} \right)^{1/7}, \tag{1-1}$$

where $\Phi_{\rm dx}$ is an order unity dimensionless number that parameterizes the amount of stellar magnetic flux that is trapped in the disk. Inside this radius, matter is channeled to the star via a funnel flow. The excess angular momentum of the accreting material is deposited in the magnetic field in the form of Maxwell torque, and then transported back to the disk. The gain of angular momentum and approximate field freezing would try to move the footpoint of the funnel-flow field lines outward.

Exterior to the truncation radius R_X, the equatorial inward drift in the accretion disk creates an angle between the stellar magnetic-field lines and the disk normal. If approximate field freezing holds as the accretion proceeds, a fraction of the field lines will develop an angle larger than 30°, when matter frozen to this flux tube becomes unstable to magnetocentrifugal fling (Blandford & Payne 1982). These field lines are thus responsible for driving a magnetohydrodynamic (MHD) wind from the disk. Since the wind removes angular momentum from the disk, the footpoints of those field lines in the disk will try to migrate inward. The radially inward press of the footpoints of the wind field lines footpoints and the radially outward press of the footpoints of the funnel-flow field lines create a magnetic X-configuration that distinguishes the model from similar variants in the literature (the historical choice of the name from the X-point of the equivalent gravitational potential in the co-rotating frame is common to many models). In quasi-steady state where radial advection into the X is balanced by the resistive diffusion of field lines out of the X, Shu et al. (1994b) estimated that enough stellar flux could be trapped in a small X-region near the inner disk edge to have large dynamical effects, namely, the truncation of the disk by a funnel flow out of the disk plane accompanied by an X-wind that carries away most of the excess angular momentum transported into the X-region.

Apart from the original numerical estimates, there are reasons to suppose that if turbulent resistivity is the source of the diffusion across magnetic field lines (Shu et al. 2007), then the fractional size of the X-region in units of R_X is given by the ratio of sound speed at the surface of the disk where the X-wind is launched to the local Keplerian speed at R_X. For the inner disk of a classical T Tauri star, the thermal sound speed is $a \sim 5$ km/s while the Keplerian speed at R_X is $v_K \sim 100$ km/s (Najita et al. 2007); thus, the ratio ϵ is a small number ~ 0.05. In an asymptotic analysis where ϵ is taken to $\rightarrow 0$, the X-wind tied to the trapped field lines in the X-region would emerge from virtually a single point in the meridional plane with a fan-like geometry. Seen by an observer rotating at the Keplertian angular frequency of R_X, gas flows along streamlines that coincide with field lines if field freezing is assumed, and both patterns of streamlines and field lines remain stationary in the corotating frame.

Viewed in this fashion, the overall problem can be broken into smaller pieces and tackled separately. Using a formulation with a precedent in the work of Lovelace

et al. (1986), Shu et al. (1988, 1994b) wrote down the mathematical equations that describe a steady state axisymmetric flow in the corotating frame (Grad & Rubin 1958, Shafranov 1966). By the method of matched asymptotic expansions, Shu et al. demonstrated the existence of an inner solution in the X-region where the flow makes a sonic transition, and an outer solution where the sound speed is formally taken to zero and the X-region shrinks down to a point. Najita & Shu (1994) computed numerically the portion of the X-wind in which the fluid velocity is sub-Alfvénic, and the governing equation is elliptic. Ostriker & Shu (1995) solved the problem of the funnel flow and the field configuration in the dead zone (in which the field lines do not depart sufficiently from disk normal to load any matter) in an approximation that treated the accretion flow onto the star as highly sub-Alfvénic. Shu et al. (1995) constructed asymptotic solutions that describe the logarithmically slow, far-wind collimation into jets. The free boundaries between various parts of the problem (funnel flow, dead zone, and X-wind) were determined by pressure balance on either side.

In this paper, we wish to address the X-wind part of the overall problem. In order for the X-wind to accelerate from rest to supersonic speeds, it must smoothly pass three surfaces on which the flow velocity is equal to the slow MHD, Alfvén, and fast MHD velocity, respectively (Heinemann & Olbert 1978, Sakurai 1985). These critical surfaces manifest themselves as singularities in the governing equation (see Weber & Davis 1967), and thus need to be handled analytically. In an axisymmetric problem, if the shapes of the streamlines are known in the meridional plane, the conserved quantities of the problem (mass to flux loading, angular momentum flux including that carried in the Maxwell stress, and Bernoulli's integral along a streamline) suffice to give a completely analytic solution, including the locations and conditions required to cross the critical surfaces smoothly. Unfortunately, the streamline distribution in the meridional plane is not known a priori but must be obtained, in principle, from a solution of the Grad-Shafranov equation (GSE). The spatial location of the critical surfaces are part of the overall solution of the GSE; indeed, they characterize the regions where this PDE is elliptic or hyperbolic. The mixed character of the GSE makes a direct numerical attack extremely difficult when self-similarity does not apply, perhaps the hardest problem in the mathematical theory of nonlinear PDEs of second-order (see Garabedian 1986). The current work sidesteps the mathematical solution of the GSE as a nonlinear PDE of second order, and approaches it instead as a much more amenable problem in variational calculus.

The rest of this paper is organized as following. In §2 we review the basic formulation in terms of a stream function and an Alfvén discriminant that yields the partial-differential equations – the so-called Grad-Shafranov and Bernoulli equations – that govern a steady, axisymmetric, X-wind flow. In §3 we write down an action whose variations with respect the stream function $\psi(\varpi, z)$ and the Alfvén discrim-

inant $\mathcal{A}(\varpi, z)$ yield, respectively, the Grad-Shafranov equation and the Bernoulli equation when the action reaches an extremum. We also perform a transformation where we replace the vertical coordinate z in cylindrical coordinates (ϖ, φ, z) by ψ. In §4, we show how to incorporate boundary conditions into the problem, as well as how to take advantage of the fact that analytic forms are known for the solutions in the near-neighborhood of the X-point and in the asymptotic regime far from the X-point (Shu et al. 1994b, 1995). In §5, we outline a practical implementation of the principle of extremal action, making use of only variations of ψ – or, more precisely, of $z(\varpi, \psi)$ in our actual working space – as the substitute to attacking the Grad-Shafranov equation, while we solve Bernoulli's equation directly for reasons that are expounded upon in this section. In §6, we present numerical results for three specific cases of mass-loading onto wind flux-tubes, finding good agreement with previous approximate solutions obtained by Shang (1998) that have been used for many different astrophysical applications (e.g., Shang et al. 1998, 2002, 2004). In §7, we summarize the recipes needed to convert the numerical solutions of §6 into practical dimensional models. We then offer our conclusions and suggestions for needed future research.

2. Basic Equations

From the fundamental parameters of the problem, we may construct units of length, time, and density as R_X, Ω_X^{-1}, and $\dot{M}_w/4\pi R_X^3\Omega_X$, respectively. By assuming axisymmetry and stationarity in a frame that is rotating with angular velocity Ω_X, we may write down the dimensionless governing equations in the above units.

$$\nabla \cdot (\rho \mathbf{u}) = 0, \tag{2-1a}$$

$$\nabla\left(\frac{1}{2}|\mathbf{u}|^2\right) + (2\mathbf{e}_z + \nabla \times \mathbf{u}) \times \mathbf{u} = -\frac{\epsilon}{\rho}\nabla\rho - \nabla V_{\rm eff} + \frac{1}{\rho}(\nabla \times \mathbf{B}) \times \mathbf{B}, \tag{2-1b}$$

$$\mathbf{B} \times \mathbf{u} = 0, \tag{2-1c}$$

$$\nabla \cdot \mathbf{B} = 0, \tag{2-1d}$$

where $\epsilon \equiv a/R_X\Omega_X$ is the sound speed measured in units of Keplerian velocity at the X-point, and is assumed to be a small parameter of the problem. The effective potential in the corotating frame is defined as

$$V_{\rm eff} = -\frac{1}{\sqrt{\varpi^2 + z^2}} - \frac{1}{2}\varpi^2 + \frac{3}{2}. \tag{2-2}$$

Here we have added a constant term to the effective potential so that its numerical value is zero at the X-point.

2.1. Constants of Motion

The continuity equation (2-1a) is satisfied identically if we define the poloidal velocity through a stream function (Shu et al. 1988, 1994a):

$$\rho u_\varpi \equiv \frac{1}{\varpi}\frac{\partial \psi}{\partial z}, \quad \rho u_z \equiv -\frac{1}{\varpi}\frac{\partial \psi}{\partial \varpi}. \tag{2-3}$$

For steady state axisymmetric flow in the corotation frame, the field freezing condition (2-1c) demands that the magnetic field and the velocity are related by (see, e.g., Mestel 1968)

$$\mathbf{B} = \beta \rho \mathbf{u}. \tag{2-4}$$

With this identification, the continuity equation (2-1a) and the absence of magnetic monopoles (2-1d) imply $\mathbf{u}\cdot\nabla\beta = 0$. In terms of the stream function, this means β is constant along each streamline, or $\beta = \beta(\psi)$.

The Euler equation describes momentum and energy balance in three spatial dimensions. If we take the component along the fluid velocity by taking the inner product of (2-1b) with $\mathbf{u}$, we obtain the Bernoulli's equation (BE) along streamlines

$$\mathbf{u}\cdot\nabla H = 0 \text{ where } \mathrm{H} \equiv \frac{1}{2}|\mathbf{u}|^2 + \epsilon^2 \ln\rho + \mathrm{V_{eff}}. \tag{2-5}$$

In other words, $H = H(\psi)$, and the energy per unit mass of an isothermal gas, including its specific enthalpy, is conserved along a streamline in the corotating frame where the flow occurs parallel to $\mathbf{B}$. Similarly, if we take the toroidal component of the Euler equation (2-1b), we obtain a third conserved quantity along stream lines, the angular momentum of the gas allowing for that part carried away by the Maxwell torque of the field:

$$J \equiv \varpi^2 + \varpi(1-\beta^2\rho)u_\varphi = J(\psi). \tag{2-6}$$

As we shall see, the determination of the conserved quantities, $H(\psi)$and $J(\psi)$, is achieved by demanding that the X-wind crosses the slow MHD and fast MHD surfaces smoothly. The loading of mass onto flux, which is governed by $\beta(\psi)$ is freely specifiable within certain limits to be detailed below.

The last component of the Euler equation describes momentum balance in the direction perpendicular to the poloidal field lines. It is the famous Grad-Shafranov equation (Heinemann & Olbert 1978, Sakurai 1985):

$$\nabla\cdot(\mathcal{A}\nabla\psi) + \frac{1}{\mathcal{A}}\left(\frac{J}{\varpi^2}-1\right)\frac{J'}{\varpi^2} + \frac{\beta^{2\prime}\{V_{\rm eff} + \epsilon^2\ln[\epsilon^2 h/(\beta^2-\varpi^2\mathcal{A})]\}}{(\beta^2-\varpi^2\mathcal{A})^2} - \frac{\epsilon^2 h'/h}{\beta^2-\varpi^2\mathcal{A}} = 0, \tag{2-7}$$

where we have rescaled Bernoulli's function as

$$H \equiv -\epsilon^2\ln(\epsilon^2 h), \tag{2-8}$$

so that h remains an order unity quantity in our calculation. Here $\mathcal{A}$ is the Alfvén discriminant defined by

$$\mathcal{A} \equiv \frac{M_A^{-2} - 1}{\varpi^2 \rho}, \tag{2-9}$$

where

$$M_A^2 \equiv \frac{\rho u^2}{B^2} = \frac{1}{\beta^2 \rho} \tag{2-10}$$

is the Alfvén Mach number. Hence $\mathcal{A}$ is positive when the total velocity is less than the Alfvén speed, and negative when the total velocity is larger than the Alfvén speed. From the form of the GSE (2-7), we see that the conserved angular momentum flux J is not freely specifiable. It is determined by the condition of smooth Alfvén transition. In order for the solution to remain continuous and differentiable, one must impose

$$J = \varpi^2 \text{ whenever } \mathcal{A} = 0. \tag{2-11}$$

The elimination of ρ in the equations in favor of $\mathcal{A}$ is based on numerical considerations, since ρ will in general vary by many orders of magnitude, while $\mathcal{A}$ only varies moderately. As we argued in the previous section, the sound speed ϵ is likely to be small. In terms of these variables, the BE takes the form

$$|\nabla\psi|^2 + \frac{1}{\mathcal{A}^2}\left(\frac{J}{\varpi^2} - 1\right)^2 + \frac{2\varpi^2\{V_{\rm eff} + \epsilon^2 \ln\left[\epsilon^2 h/(\beta^2 - \varpi^2\mathcal{A})\right]\}}{(\beta^2 - \varpi^2\mathcal{A})^2} = 0. \tag{2-12}$$

2.2. The Cold Limit

With $\mathcal{A}$ implicitly defined in the BE (2-12), the GSE is a PDE of mixed type, which demands different numerical methods in different regions (see Heinemann & Olbert 1978 and Appendix A). There are three relevant signal speeds (which we term sonic, slow, and fast in the appendix) involved in an MHD flow (see Jackson 1975 or Shu 1992). The loci where the poloidal fluid speed equals those signal speeds separate the flow into four regions. As the poloidal velocity exceeds the sonic speed, the governing GSE changes from elliptic to hyperbolic. A wise strategy might start with the search of appropriate boundary conditions in the disk where $u_p^2 = 0$, and at the sonic surface (whose location is still undetermined), followed by a standard scheme (e.g., relaxation) to obtain the interior solution. Beyond the sonic surface, the GSE becomes hyperbolic. The boundary condition on the sonic surface now serves as the initial condition, which we use to integrate forward along characteristics toward the slow surface. We then follow similar procedures to obtain solutions from the slow surface to the fast surface, and beyond.

A significant simplification can be achieved when the sound speed is negligible, as in the outer problem of the X-wind (see §4 of Shu et al. 1994b). The governing

equations are treated as power series expansion in ϵ. The leading term in the GSE (2-7) and the BE (2-12) are

$$\nabla \cdot (\mathcal{A}\nabla\psi) + \frac{1}{\mathcal{A}}\left(\frac{J}{\varpi^2} - 1\right)\frac{J'}{\varpi^2} + \frac{\beta^{2\prime}V_{\rm eff}}{(\beta^2 - \varpi^2\mathcal{A})^2} = 0, \tag{2-13a}$$

$$|\nabla\psi|^2 + \frac{1}{\mathcal{A}^2}\left(\frac{J}{\varpi^2} - 1\right)^2 + \frac{2\varpi^2 V_{\rm eff}}{(\beta^2 - \varpi^2\mathcal{A})^2} = 0. \tag{2-13b}$$

Notice the lowest order term in H vanishes independent of the form of h. In this limit, both the sonic speed and the slow speed reduce to zero, and the first elliptic and hyperbolic parts of the flow shrink down to the X-point. We are thus spared the vicissitudes of this portion of the problem. Once the fluid leaves the X-region (with poloidal velocity greater than the slow speed), it proceeds to the fast surface, where the governing equation becomes hyperbolic.

Najita & Shu (1994) solved the GSE in the sub-Alfvénic region. By introducing a generalized coordinate system, they were able to map the location of the Alfvén surface to a known location, and determine the functional form of $\beta(\psi)$ based on the position and shape of the Alfvén surface. Their numerical scheme to find $\beta(\psi)$ by iteration encountered a systematic "drift problem", however, and an artificial "Alfvén seam" was invented to cope with this difficulty.

In a later treatment by Shang (1998), $\beta(\psi)$ was specified in advance, limited in its functional form by considerations of how the gas exits the X-region, an analysis that we repeat in §4.2 (see also §5). The GSE was not solved as a PDE, but rather as an error estimator in a Weber-Davis type of analysis, where ψ as a trial function of spatial location is obtained by interpolating between the known analytic forms in the X-point neighborhood (see §4.1) and at asymptotic infinity (see §4.3). The interpolation formula has a number of degrees of freedom, which are adjusted to give "least error" in some sense when the trial solution for ψ is substituted back into the GSE. The rest of the problem, including the constraints of the conserved quantities and smooth passage through the Alfvén and fast surfaces, are performed exactly. She verified the result derived by Goldreich and Julian (1970) that passage through the Alfvén surface is automatic in such a scheme if one has guaranteed it through the fast surface. In fact, §5.2 demonstrates the falsity of the frequent claim made otherwise in the literature that $J(\psi)$ is set at the Alfvén surface; the claim holds only if one already has a solution such that the wind passes smoothly through the fast surface.

3. Variational Principle

Based on the above arguments, the X-wind is a fierce mathematical beast, and a direct numerical attack is unlikely to subdue it fully. To construct a global solution of

the X-wind that accelerates elements of plasma from the disk to super-magnetosonic speeds, we must resort to a different approach. Consider the following action written down by inspection:[1]

$$S = \int \left\{ \frac{1}{2}\mathcal{A}|\nabla\psi|^2 - \frac{1}{2\mathcal{A}}\left(\frac{J}{\varpi^2} - 1\right)^2 + \frac{V_{\rm eff} + \epsilon^2 \ln[\epsilon^2 h/(\beta^2 - \varpi^2\mathcal{A})] - \epsilon^2}{\beta^2 - \varpi^2\mathcal{A}} \right\} d^3x, \tag{3-1}$$

It is straight forward to demonstrate that variation against ψ yields the GSE (2-7), while variation against $\mathcal{A}$ gives the BE (2-12). The challenges of constructing solutions to a nonlinear PDE of mixed type is now transformed to tuning trial functions of ψ and $\mathcal{A}$ until a local extremum of the action (3-1) is reached.

To formulate a scheme that is easy to implement numerically, we consider a change of independent variables from the usual cylindrical coordinates

$$(\varpi, z, \varphi) \rightarrow (\varpi, \psi, \varphi).$$

For a given value of ψ, the functional form of $z(\varpi)$ determines the shape of the given streamline, and $\mathcal{A}(\varpi)$ offers information on the velocity distribution along that streamline. Written in these new coordinates, and taking the cold limit as $\epsilon \rightarrow 0$, the action reads

$$S = 2\pi \iint \left\{ \frac{1}{2}\mathcal{A}\left(\frac{\partial z}{\partial \psi}\right)^{-1}\left[1 + \left(\frac{\partial z}{\partial \varpi}\right)^2\right] - \frac{1}{2\mathcal{A}}\frac{\partial z}{\partial \psi}\left(\frac{J}{\varpi^2} - 1\right)^2 + \frac{\partial z}{\partial \psi}\frac{V_{\rm eff}}{\beta^2 - \varpi^2\mathcal{A}} \right\} \varpi d\psi d\varpi \tag{3-2}$$

Since $\mathcal{A}$ only enters the action as a constraint rather than a dynamic variable (i.e., its derivative is absent in the action), variation with respect $\mathcal{A}$ yields the BE as before, but now written in a different set of coordinates,

$$\left(\frac{\partial z}{\partial \psi}\right)^{-2}\left[1 + \left(\frac{\partial z}{\partial \varpi}\right)^2\right] + \frac{1}{\mathcal{A}^2}\left(\frac{J}{\varpi^2} - 1\right)^2 + \frac{2\varpi^2 V_{\rm eff}}{(\beta^2 - \varpi^2\mathcal{A})^2} = 0 \tag{3-3}$$

Variation with respect to z gives

$$\begin{aligned} \delta S_z = 2\pi \iint \Bigg\{ & -\frac{1}{2}\mathcal{A}\left(\frac{\partial z}{\partial \psi}\right)^{-2}\frac{\partial \delta z}{\partial \psi}\left[1 + \left(\frac{\partial z}{\partial \varpi}\right)^2\right] + \mathcal{A}\left(\frac{\partial z}{\partial \psi}\right)^{-1}\left(\frac{\partial z}{\partial \varpi}\right)\frac{\partial \delta z}{\partial \varpi} \\ & -\frac{1}{2\mathcal{A}}\frac{\partial \delta z}{\partial \psi}\left(\frac{J}{\varpi^2} - 1\right)^2 + \frac{\partial \delta z}{\partial \psi}\frac{V_{\rm eff}}{\beta^2 - \varpi^2\mathcal{A}} + \frac{\partial z}{\partial \psi}\frac{V_{\rm eff,z}}{\beta^2 - \varpi^2\mathcal{A}}\delta z \Bigg\} \varpi d\psi d\varpi. \end{aligned}$$

[1]In their pioneering development of magnetized stellar winds in a Grad-Shafranov formalism, Heinemann & Olbert (1978) noted in passing that the resultant equations could be derived from a principle of least action, which differs in detailed form from that used in this paper, but is in the same spirit. However, they, and subsequent workers who have made similar observations, did not exploit the principle to obtain actual wind solutions.

Integrating by parts, we have

$$\begin{aligned}\delta S_z = 2\pi \int \left\{ -\frac{1}{2}\mathcal{A}\left(\frac{\partial z}{\partial \psi}\right)^{-2}\left[1+\left(\frac{\partial z}{\partial \varpi}\right)^2\right] - \frac{1}{2\mathcal{A}}\left(\frac{J}{\varpi^2}-1\right)^2 + \frac{V_{\rm eff}}{\beta^2-\varpi^2\mathcal{A}}\right\}\varpi\delta z\Big|_{\psi=0}^{\psi=1} d\varpi \\ +2\pi\int \mathcal{A}\left(\frac{\partial z}{\partial \psi}\right)^{-1}\left(\frac{\partial z}{\partial \varpi}\right)\delta z\varpi\Big|_{\varpi=1}^{\varpi=\infty} d\psi \\ +2\pi\iint \frac{\partial}{\partial\psi}\left\{\frac{1}{2}\mathcal{A}\left(\frac{\partial z}{\partial \psi}\right)^{-2}\left[1+\left(\frac{\partial z}{\partial \varpi}\right)^2\right] + \frac{1}{2\mathcal{A}}\left(\frac{J}{\varpi^2}-1\right)^2 - \frac{V_{\rm eff}}{\beta^2-\varpi^2\mathcal{A}}\right\}\varpi\delta z d\psi d\varpi \\ +2\pi\iint\left\{\frac{\partial z}{\partial\psi}\frac{\varpi V_{\rm eff,z}}{\beta^2-\varpi^2\mathcal{A}} - \frac{\partial}{\partial\varpi}\left[\mathcal{A}\left(\frac{\partial z}{\partial\psi}\right)^{-1}\left(\frac{\partial z}{\partial\varpi}\right)\varpi\right]\right\}\delta z d\psi d\varpi.\end{aligned}$$

Since we specify the boundary condition $z=0$ on $\psi=0$, and $z=Z(\varpi)$ on $\psi=1$, where $Z(\varpi)$ is a known function, we see that δz vanishes on these two boundaries. As we shall see later (see 48; 49), the solution near the X-point and asymptotically can be constructed analytically. Thus δz also vanishes when $\varpi=1$ and $\varpi\to\infty$ in our variational scheme, and both surface terms vanish in the above expression. In order for the action to be stationary against any choice of δz, the solution must satisfy the Euler Lagrange equation,

$$\begin{aligned}\frac{\delta S}{\delta z} = \frac{\partial}{\partial\psi}\left\{\frac{1}{2}\mathcal{A}\left(\frac{\partial z}{\partial\psi}\right)^{-2}\left[1+\left(\frac{\partial z}{\partial\varpi}\right)^2\right] + \frac{1}{2\mathcal{A}}\left(\frac{J}{\varpi^2}-1\right)^2 - \frac{V_{\rm eff}}{\beta^2-\varpi^2\mathcal{A}}\right\}\varpi \\ +\frac{\partial z}{\partial\psi}\frac{\varpi}{\beta^2-\varpi^2\mathcal{A}}\frac{\partial V_{\rm eff}}{\partial z} - \frac{\partial}{\partial\varpi}\left[\mathcal{A}\left(\frac{\partial z}{\partial\psi}\right)^{-1}\left(\frac{\partial z}{\partial\varpi}\right)\varpi\right] = 0. \qquad (3\text{-}4)\end{aligned}$$

Dividing both sides by ϖ, we can simplify the Euler-Lagrange equation (3-4) to obtain

$$\begin{aligned}-\frac{1}{2}\frac{\partial\mathcal{A}}{\partial\psi}\left\{\left(\frac{\partial z}{\partial\psi}\right)^{-2}\left[1+\left(\frac{\partial z}{\partial\varpi}\right)^2\right] + \frac{1}{\mathcal{A}^2}\left(\frac{J}{\varpi^2}-1\right)^2 + \frac{2\varpi^2 V_{\rm eff}}{(\beta^2-\varpi^2\mathcal{A})^2}\right\} \\ +\frac{1}{\mathcal{A}}\left(\frac{J}{\varpi^2}-1\right)\frac{J'}{\varpi^2} + \frac{\beta^{2\prime}V_{\rm eff}}{(\beta^2-\varpi^2\mathcal{A})^2} - \frac{1}{\varpi}\left(\frac{\partial z}{\partial\psi}\right)^{-1}\frac{\partial}{\partial\varpi}\left[\mathcal{A}\left(\frac{\partial z}{\partial\varpi}\right)\varpi\right] \\ +\left(\frac{\partial z}{\partial\psi}\right)^{-1}\frac{\partial}{\partial\psi}\left\{\mathcal{A}\left(\frac{\partial z}{\partial\psi}\right)^{-1}\left[1+\left(\frac{\partial z}{\partial\varpi}\right)^2\right]\right\} = 0. \qquad (3\text{-}5)\end{aligned}$$

We notice that the coefficient of $\partial\mathcal{A}/\partial\psi$ is simply the BE, which vanishes at a local extremum of the action. One may easily check that the other terms yield the conventional GSE, but written in our new coordinates.

4. Boundary Conditions

4.1. X-point

With the new coordinates, the computational domain is bounded by $\psi \in [0,1]$ and $\varpi \in [1,\infty)$. The X-point in these coordinates is a singularity given by $\varpi = 1$ for all values of ψ. Fortunately, we have analytic solutions there. From this point onward, we shall work with a scaled Alfvén discriminant

$$\chi \equiv \frac{\mathcal{A}}{\beta^2}. \tag{4-1}$$

This function has the advantage of remaining finite even when β diverges. For a given functional form of β (which tells us how matter is loaded onto the field lines), the Alfvén discriminant has the series expansion in $\varpi - 1$.

$$\chi_X = 1 + \chi_1(\psi)(\varpi - 1) + \chi_2(\psi)(\varpi - 1)^2 + ..., \tag{4-2}$$

Here a subscript X reminds us that this series solution is valid near the X-point. In order to match asymptotically onto the outer limit of the inner problem (Shu et al. 1994b), the density $\rho \equiv \beta^{-2}(1 - \varpi^2\chi)^{-1}$ must diverge as $(\varpi - 1)^{-2}$ near the X-point. This requirement translates to $\chi_1 = -2$ for all values of ψ. Similarly, for the coordinate z (now a dependent variable), we expand it as,

$$z_X = z_1(\psi)(\varpi - 1) + z_2(\psi)(\varpi - 1)^2 + ... \tag{4-3}$$

Notice that the Jacobian near the X-point is

$$\sqrt{g} = z_1'(\varpi - 1) \text{ as } \varpi \to 1.$$

which is expected since the entire line of $\psi \in [0,1]$ is mapped into a single point, and the Jacobian must vanish in this situation. Substituting the series expansion into the GSE (3-5) in the transformed coordinates, the lowest order is $(\varpi - 1)^{-2}$.

$$\frac{\partial}{\partial\psi}\left[\frac{\beta}{z_1'}\left(1 + z_1^2\right)\right] = 0,$$

which has the solution

$$z_1 = \tan\vartheta, \qquad \vartheta = \frac{1}{K}\int_0^\psi \beta d\psi. \tag{4-4}$$

If we assume that the upper boundary of the X-wind ($\psi = 1$) near the X-point forms an angle of θ_X with the x axis, we have

$$\tan\theta_X \approx \frac{z}{\varpi - 1}\Big|_{\chi\to 1} = z_1(\psi = 1) = \tan\frac{1}{K}\int_0^1 \beta d\psi.$$

Thus, the integration constant is given by

$$K = \frac{\bar{\beta}}{\theta_X}, \qquad \bar{\beta} = \int_0^1 \beta d\psi. \tag{4-5}$$

Substituting back into the Bernoulli's equation allows us to solve for χ_2,

$$\chi_2 = 3 - \frac{\sqrt{4\cos^2\vartheta - 1}}{K\beta\cos^2\vartheta} \tag{4-6}$$

For better numerical accuracy, we carry out the computation to next order. The next term in the series expansion of the GSE is $O[(\varpi - 1)^{-1}]$:

$$\frac{\partial^2 \mathcal{Q}}{\partial \vartheta^2} + \mathcal{Q} = \sin\vartheta,$$

where $\mathcal{Q} = z_2 \cos^3\vartheta$. Given the boundary condition $z = 0$ at $\psi = 0$ for all values of χ, the above equation may be solved to give

$$z_2 = \frac{1}{2}\sec^2\vartheta(q\tan\vartheta - \vartheta). \tag{4-7}$$

The integration constant q can be determined by expanding the upper boundary near the X-point. Substituting into the BE, we can determine the last term without the knowledge of J as

$$\chi_3 = \frac{\cos^2\vartheta - 2 + \tan\vartheta(q\tan\vartheta - \vartheta)}{2K\beta\cos^2\vartheta\sqrt{4\cos^2\vartheta - 1}} + \frac{\sqrt{4\cos^2\vartheta - 1}(4 - q\sec^2\vartheta)}{2K\beta\cos^2\vartheta} - 4. \tag{4-8}$$

4.2. Specifying Mass Loading and Difficulties with the Boundary Layer

Since the X-wind is driven magnetocentrifugally, one would naively expect that it is bounded away from the polar axis (at least in the immediate vicinity of the X-point) by some curve which intersects the disk. In the outer limit of the inner problem (see eq. 3.10d of Shu et al. 1994b), the gas pressure $p = \epsilon^2\rho$ takes the form

$$p \to \left[\frac{\bar{\beta}}{\vartheta_x(0)\beta}\right]\sigma^{-2}(4\cos^2\vartheta - 1)^{-1/2}, \text{ as } \sigma \to \infty,$$

where $\tan\vartheta = z/(\varpi - 1)$. As $\vartheta_x \to \pi/3$ (which is the critical angle for the last matter carrying streamline), the pressure diverges unless

$$\beta \propto (4\cos^2\vartheta - 1)^{-1/2}, \text{ as } \psi \to 1.$$

Substitute this functional form into the lowest order equation (4-4), finite magnetic field and pressure on the last streamline demands

$$\beta \propto (1 - \psi)^{-1/3}, \text{ as } \psi \to 1. \tag{4-9}$$

The divergence of β should not come as a surprise. Recall that the last streamline is defined to be the boundary between the X-wind and the dead zone. To ensure analyticity across this boundary, we must have $\rho \to 0$ as $\psi \to 1$. Now since neither the magnetic field nor the velocity become singular, we must take $\beta \to \infty$ on that last streamline, so that the product $\beta^2\rho^2 = B^2/u^2$ remains finite. With this limit in place, we see that the rescaled Alfvén discriminant

$$\chi = \frac{1 - 1/\beta^2\rho}{\varpi^2} \to \frac{1}{\varpi^2}$$

remains positive for all points along the last streamline. In other words, the flow on the last streamline is always sub-Alfvénic, since the Alfvén speed is infinite there. This behavior of the last streamline requires a double limiting procedure if we were to accurately construct the asymptotic solution on that interface. We speculate that this difficulty is an indication that the last streamline needs to be treated as a boundary layer. This speculation is reinforced by the fact that the last X-wind streamline is the outer bounding surface to a sheet of axisymmetric current defined by opened stellar field lines that reverse poloidal directions as the current sheet is crossed and we find ourselves in the dead zone of the overall X-wind/funnel-flow configuration (see Fig. 1). Until we actually construct such a boundary-layer/current-sheet theory, we adopt a simple modification to deal with the problem: we truncate the formal wind solution at some $\psi_1 < 1$, below which J and β remain finite. We then add the part between ψ_1 and 1 to the dead zone fields of the problem, i.e., treat the last few streamlines as opened vacuum fields and impose the pressure balance condition at ψ_1.

4.3. Asymptotic Solution

The asymptotic solution at large distances from the X-point was constructed by Shu et al. (1995). In particular, for a wind reaching more or less constant terminal velocity, its density scales roughly as $\rho \propto \varpi^{-2}$, and the Alfvén discriminant $\chi \to -1/\beta^2\rho\varpi^2$ is a slowly varying function of r. By ignoring all radial derivatives compared to angular derivatives, the GSE and the BE admit solutions of the form

$$\chi = -1/\beta C, \qquad \sin\theta = \mathrm{sech}[\mathrm{C}^{-1}\mathrm{I}(\mathrm{C},\psi)], \qquad \mathrm{I}(\mathrm{C},\psi) = \int_0^\psi \frac{\beta \mathrm{d}\psi}{\sqrt{2\mathrm{J} - 3 - 2\mathrm{C}\beta}}, \tag{4-10}$$

where θ is the usual polar angle in spherical coordinates, and C is a "constant of integration" that vary slowly in r. In an inertial frame, the wind reaches a terminal velocity given by

$$v_w = (2J - 3 - 2C\beta)^{1/2}. \tag{4-11}$$

To determine the constant C, we impose pressure balance between the X-wind and the dead zone. Since the dead zone field lines carry no inertia, they do not develop

a toroidal component, and the poloidal field satisfies the vacuum equation (Ostriker & Shu1994). Asymptotically, we do not expect the field lines to pinch toward the rotational axis since the hoop stress is vanishingly small (Shu et al. 1995). For simplicity, we assume the boundary layer deviates only slightly from a cylindrical surface at the asymptotic infinity (an assumption which shall be checked a posteriori for consistency). For any given (large) value of r, we can approximate the boundary locally by $\varpi = \text{const}$. Then a particular solution is $\mathbf{B} = B_{\rm hc}\hat{\mathbf{z}}$. For the hollow-cone region to trap the same amount of *net* flux as the wind part and have a cross-sectional area of $\pi\varpi_{\rm hc}^2$, we have

$$B_{\rm hc} = \frac{2\phi_{\rm hc}\bar{\beta}}{\varpi_{\rm hc}^2},$$

where $\phi_{\rm hc}$ is a number ranging from 1 to 3 depending on the fraction of closed field lines in the dead zone (compare Fig. 1 of this paper with Fig. 1 of Shu et al. 2001). The maximal case $\phi_{\rm hc} = 3$ has three times as many field lines as the minimal case $\phi_{\rm hc} = 1$, but the extra field lines cancel in oppositely directed pairs and contribute no net flux. The overall solution does not depend sensitively on the number $\phi_{\rm hc}$, and we take $\phi_{\rm hc}$ henceforth to be unity as illustrated in Figure 1 of the current paper.

In contrast, the wind region is dominated by the toroidal field

$$B_{w,\varphi} = \beta\rho u_\varphi = -\frac{J - \varpi^2}{\varpi^3\chi\beta} \to -\frac{C}{\varpi}.$$

The poloidal field $B_{w,p} = \beta\rho v_w \propto 1/\varpi^2$ is much weaker in this limit. By equating the magnetic pressures on both sides of the boundary, $B_{\rm hc}^2 = B_{w,\varphi}^2$, we obtain

$$C = \frac{2\bar{\beta}}{\varpi_{\rm hc}} = \frac{2\bar{\beta}}{r}\cosh[C^{-1}I(C,1)], \tag{4-12}$$

which implicitly defines $C(r)$. Since I only depends very weakly on C, this expression shows that $C \to 0$ logarithmically as $r \to \infty$. Notice that this limiting behavior of C ensures that $\varpi_{\rm hc}$ deviates from a constant only logarithmically slowly, which validates our assumption on the geometry of the boundary layer. Written in our coordinates, the asymptotic geometry of each streamline is given by

$$z = \varpi\sinh[C^{-1}I(C,\psi)]. \tag{4-13}$$

In other words, each streamline is approximately radial, with a logarithmic collimation toward the axis.

With $\rho \to C/\beta\varpi^2$ and $v_w \to$ constant, the poloidal and toroidal Alfvén speeds are given by

$$v_{A,p}^2 = B_p^2/\rho \to C\beta v_w^2/\varpi^2, \qquad v_{A,\varphi}^2 = B_\varphi^2/\rho \to C\beta. \tag{4-14}$$

Thus the Alfvén speed is dominated by the toroidal component, which decreases logarithmically. This means that the (poloidal) terminal velocity is super-fast in

the asymptotic regime, and the wind has to make a fast mode transition along each streamline. The above analysis simply reiterates the claims made in Appendix A that the asymptotic behavior of the flow is governed by a hyperbolic differential equation.

5. Global Solutions

As a particular example, let us suppose that diffusive mass loading onto field lines in the X-region produces a β function which has the form

$$\beta = \frac{2}{3}\bar{\beta}(1-\psi)^{-1/3}. \tag{5-1}$$

It is easy to verify that $\int_0^1 \beta d\psi = \bar{\beta}$. To be definite, let us also assume that the upper boundary of the X-wind near the X-point forms the maximum angle $\vartheta_X = \pi/3$ with the equatorial plane in order for magnetocentrifugal acceleration to operate. The $O[(\varpi-1)^{-2}]$ solution (4-4) takes the form

$$z_1 = \tan\vartheta = \tan\frac{\pi}{3}\big[1-(1-\psi)^{2/3}\big]. \tag{5-2}$$

In fact we have chosen a very special value for the opening angle. Recall that the formal boundary between the X-wind and the dead zone is characterized by vanishing ρ with finite magnetic field. That results in $\beta \to \infty$ and $\chi = \varpi^{-2}$. If ϑ_X were smaller than $\pi/3$, one may check that the boundary condition $\chi = \varpi^{-2}$ agrees with the series solution of §4.1 to the second order for all values of q. This integration constant is computed by expanding the shape of the last streamline near the X-point. However, when $\vartheta_X = \pi/3$, the series solution agrees with the boundary condition only if the quantity q in equation (4-7) satisfies

$$q = \frac{1}{3}\left(\frac{7}{4} + \frac{\pi}{\sqrt{3}}\right).$$

If $\vartheta_X > \pi/3$, the solution becomes discontinuous. This behavior is consistent with our physical intuition. When the flow is cold, the upper boundary of the X-wind is imposed by pressure balance. As one eases up the external pressure, ϑ_X increases. However, even when the external pressure drops to zero, the matter carrying streamlines are confined to $\vartheta \le \pi/3$, since it is the boundary where centrifugal effects can overcome gravity. At least near the X-point, there is no freedom to choose the shape of the last streamline. Any excursion across this boundary requires additional pressure support from the X-wind, which calls for a warm rather than cold outflow.

In the particular example we are studying here, the second order coefficient for z becomes

$$z_2 = \frac{1}{2}\sec^2\vartheta\left[\left(\frac{7}{12} + \frac{\pi}{3\sqrt{3}}\right)\tan\vartheta - \vartheta\right]. \tag{5-3}$$

For numerical tractability, we place the boundary layer at $\psi = 0.99$. Given the choice of mass loading in equation (5-1), the β function is not much larger than unity there.

5.1. Fixing the Free Function $J(\psi)$

The BE (2-13b) is actually a quartic algebraic equation for the Alfvén discriminant once the shape of the streamlines are known. The Alfvén surface here is not a real singularity of the equation; it simply ensures that $\chi = 0$ is a solution when $J = \varpi^2$. In other words smooth crossing of the Alfvén surface does not uniquely determine the value of J. To see this, let us define

$$\mathcal{L} = \varpi \rho u_\varphi = -\frac{1}{\beta^2 \chi}\left(\frac{J}{\varpi^2} - 1\right).$$

It is always negative and asymptotes to zero for the wind since the magnetic field lines form a trailing spiral. The BE can be written as

$$(|\nabla\psi|^2 + \mathcal{L}^2)(\beta^2\mathcal{L} + J - \varpi^2)^2 + 2\varpi^2 V_{\rm eff}\mathcal{L}^2 = 0. \tag{5-4}$$

As long as J is larger than some critical value, there are always real and finite solutions to this equation, which means the Alfvén surface is automatically crossed. On the other hand, the fast point is a real critical point for the BE. A smooth fast mode transition demands the BE to have a double root at the critical point (see Fig 2). That means not only does the left hand side of (5-4) need to vanish, its derivative with respect to $\mathcal{L}$ must vanish as well.

After some algebra, these requirements can be written as

$$\mathcal{L} = |\nabla\psi|^{2/3}(J - \varpi^2)^{1/3}\beta^{-2/3}. \tag{5-5}$$

This expression is simply a statement that at the fast point, the poloidal fluid velocity is equal to the magnetosonic speed, which for $\epsilon = 0$ is equal to the total Alfvén speed. Notice that both equations (5-4) and (5-5) are automatically satisfied by $\mathcal{L} = (J - \varpi^2) = 0$. This solution, however, is unphysical since it has a discontinuity on the Alfvén surface when $\chi = 0$. Substituting equation (5-5) back in to the BE (5-4), we have

$$\left[|\nabla\psi|^{2/3}\beta^{4/3} + (J - \varpi^2)^{2/3}\right]^3 + 2\varpi^2 V_{\rm eff} = 0. \tag{5-6}$$

For a given value of J, the solutions to this equation give the locations where the BE has degenerate roots. If $J < J_c$, equation (5-6) has no roots in the super-Alfvén region ($\varpi^2 > J$). If $J > J_c$, then equation (5-6) has two roots in the super-Alfvén part of the flow. The desired solution is obtained when $J = J_c$, and there is only one double root occurring at the fast mode transition point (see Fig. 2).

5.2. Interpolation Schemes and Numerical Strategy

Our strategy is then to find interpolations between the X-point solution in §4.1 and the asymptotic solution of §4.3 so that the action (3-2) is extremized. Since the action involves an integral extending to $r \to \infty$, and the streamlines are approximately radial, in general the action integral is infinite. In the X-wind problem, however, the assumption of stationarity is an approximation that must fail physically at very large distances from the X-point. If the flow extends all the way to spatial infinity, then steady state cannot be established in finite time. To make the practical aspect of this problem manageable, we opt to truncate the action integral at some finite spatial surface, and assume that the solution is identical to the asymptotic solution beyond that point. Then the interpolation requires the intermediate solution to join smoothly on to the asymptotic solution at the boundary. Since the parameter C that appears in the asymptotic solution is purely a function of r, it is natural to choose the boundary surface at $r = r_0 < \infty$. Thus, along a given streamline labeled by ψ, the action involves an integral over the range $\varpi \in [1, \varpi_\infty]$, where

$$\varpi_\infty = \frac{2\bar{\beta}}{C} \frac{\cosh[C^{-1} I(C, 1)]}{\cosh[C^{-1} I(C, \psi)]} \tag{5-7}$$

Here I is the integral defined in equation (4-10), and the asymptotic value of z is given by

$$z_\infty(\varpi, \psi) = \varpi_\infty \sinh\left[C^{-1} I(C, \psi)\right], \tag{5-8}$$

Since the asymptotic behavior of the streamlines are predominantly radial with a logarithmic collimation toward the pole, we may approximate them by linear functions. There is a large class of basis functions in which $z(\psi, \varpi)$ can be expanded. To avoid unphysical oscillations introduced by higher order polynomial interpolations, we approximate z by a cubic spline such that the second derivative $z_{\varpi\varpi}$ is a continuous piecewise linear function.

$$z_{\varpi\varpi} = f_i + (\varpi - \varpi_i) \frac{f_{i+1} - f_i}{\varpi_{i+1} - \varpi_i}, \text{ for } \varpi_\mathrm{i} \le \varpi < \varpi_\mathrm{i+1}, \tag{5-9}$$

where $i = 0...N-1$, with $\varpi_0 = 1$ and $\varpi_N = \varpi_\infty$. The boundary conditions on $z_{\varpi\varpi}$ read

$$f_0 = 2z_2, \qquad f_N = 0. \tag{5-10}$$

Direct integration yields (36)

$$z = a y_i + b y_{i+1} + c f_i + d f_{i+1}, \tag{5-11}$$

$$z_\varpi = \frac{y_{i+1} - y_i}{\varpi_{i+1} - \varpi_i} - \frac{3a^2 - 1}{6}(\varpi_{i+1} - \varpi_i) f_i + \frac{3b^2 - 1}{6}(\varpi_{i+1} - \varpi_i) f_{i+1}, \tag{5-12}$$

where

$$a \equiv \frac{\varpi_{i+1} - \varpi}{\varpi_{i+1} - \varpi_i}, \qquad b \equiv 1 - a = \frac{\varpi - \varpi_i}{\varpi_{i+1} - \varpi_i},$$

$$c \equiv \frac{1}{6}(a^3 - a)(\varpi_{i+1} - \varpi_i)^2, \qquad d \equiv \frac{1}{6}(b^3 - b)(\varpi_{i+1} - \varpi_i)^2,$$

and $y_i \equiv z(\varpi_i)$ for that particular streamline. The y_i are determined by demanding z_ϖ is continuous throughout the domain. Explicitly,

$$\frac{\varpi_i - \varpi_{i-1}}{6} f_{i-1} + \frac{\varpi_{i+1} - \varpi_{i-1}}{3} f_i + \frac{\varpi_{i+1} - \varpi_i}{6} f_{i+1} = \frac{y_{i+1} - y_i}{\varpi_{i+1} - \varpi_i} - \frac{y_i - y_{i-1}}{\varpi_i - \varpi_{i-1}}, \quad (5\text{-}13)$$

which is a set of $N-2$ linear equations for the N y_i. The boundary conditions $y_0 = 0$ and $y_N = z_\infty$ close the equations, and allows unique determination of y_i once f_i are given. Since we have information on the slope of the solution on both boundaries, they impose two further constraints

$$z_1 = \frac{y_1 - y_0}{\varpi_1 - \varpi_0} - \frac{1}{3}(\varpi_1 - \varpi_0) f_0 - \frac{1}{6}(\varpi_1 - \varpi_0) f_1, \quad (5\text{-}14)$$

$$z_{\infty,\varpi} = \frac{y_N - y_{N-1}}{\varpi_N - \varpi_{N-1}} + \frac{1}{6}(\varpi_N - \varpi_{N-1}) f_{N-1} + \frac{1}{3}(\varpi_N - \varpi_{N-1}) f_N. \quad (5\text{-}15)$$

To demonstrate the principles, we choose $N = 3$, so that all the f_i are constrained. For a given set of ϖ_i, the equations (5-13), (5-14), and (5-15) form a set of four linear equations, which can be solved by standard means. We also define ϖ_2 by

$$\frac{\varpi_2 - \varpi_1}{\varpi_1 - 1} = \frac{\varpi_\infty - \varpi_2}{\varpi_2 - \varpi_1}, \quad (5\text{-}16)$$

i.e., we demand that the interval between interpolation points to increase exponentially. Thus the shape of each streamline is parameterized by a single variable, ϖ_1.

The action integral and the asymptotic solution can be treated as solutions to a set of simultaneous "ordinary" differential equations

$$\frac{dS}{d\psi} = \int_1^{\varpi_\infty(\psi)} L\varpi d\varpi, \qquad \frac{dI}{d\psi} = \frac{\beta}{\sqrt{2J(\psi) - 3 - 2C\beta(\psi)}}, \quad (5\text{-}17)$$

subject to the boundary conditions

$$S(0) = 0, \qquad I(0) = 0.$$

Here L represents the Lagrangian appearing in the action (3-2). For each value of ψ, to compute the right hand side of equation (5-17), one needs the values of $\varpi_1(\psi)$, $I(\psi)$ and $I(\psi_1)$, where $\psi_1 = 0.99$ is the label of the boundary layer discussed in §4.2. Ideally, one would like to specify the shape of the last streamline by fixing the values of $\varpi_1(\psi_1)$ and $I(\psi_1)$ as boundary conditions, and vary the function $\varpi_1(\psi)$ in a constrained manner to achieve a local extremum of the action. In practice, we find it more convenient to implement a scheme where only $\varpi_1(\psi_1)$ is given, and $I(\psi_1)$ is determined as an eigenvalue. This approach allows more freedom in the parameter search for the desired $\varpi_1(\psi)$. With each streamline fully parameterized, one can

proceed to determine the necessary value of $J(\psi)$ that allows a smooth fast mode transition according to the procedure outlined in §5.1.

Once $J(\psi)$ and $I(\psi)$ are both known, we can easily solve the BE (2-13b) as an algebraic equation along each streamline for $\mathcal{L}$ using standard techniques such as Laguerre's method (see Press et al. 1992). In particular, note that we do *not* actually use the extremal property of the action principle with respect to $\mathcal{A}$ to attack the Bernoulli equation, but effect direct solutions of it instead. Increased numerical accuracy constitutes only one reason for a mixed procedure, where we do find the extremal action through variations of ψ, or equivalently, through variations of $z(\varpi, \psi)$, as a substitute for solving the Grad-Shafranov equation. There is a yet more practical reason. It turns out the the correct solution sits on a saddle, where the extremal action is minimized by variations of ψ but maximized by variations of $\mathcal{A}$. This combination makes a numerical search for the extremal action extremely difficult to execute in practice, perhaps even impossible, if the search is carried out in the double-function space of allowable ψ and $\mathcal{A}$.

One further obstacle to overcome is that the action integral (3-2) is logarithmically divergent at the X-point. Recall that the Jacobian of the coordinate transformation vanishes at the X-point since it maps the entire axis of $\varpi = 1$ onto a single point. A series expansion of the Lagrangian using the series solution of section §4.1 shows that it diverges as

$$L_* = \frac{K\beta}{2(\varpi - 1)}. \tag{5-18}$$

Fortunately, this term does not enter into the variation scheme, and we may safely remove it as a counter term from the Lagrangian, as is the standard practice in quantum-field theory.

Finally, the function $\varpi_1(\psi)$ is modeled by a Hyman filtered spline (21) interpolating over evenly spaced control points $\psi_i \in [0, \psi_1]$. The values of ϖ_1 at these control points, $\varpi_1(\psi_i)$, are the parameters we can adjust in our variation scheme. We restrict the parameter space to that satisfies the condition that the streamlines do not cross and that each streamline is monotonic. We then adopt a genetic algorithm to search for a set of $\varpi_1(\psi_i)$ that gives a local extremum of the action (3-2).

6. Numerical Results

We compute the streamlines for three cases of average mass loading corresponding to $\bar{\beta} = 1, 2, 3$. In each case, we place the outer boundary of the computational domain at a constant radius so that it intersects the last streamline at $\varpi_\infty(\psi_1) = 20$ (which yields $C = 0.1\bar{\beta}$). After a multidimensional search, we locate the desired set of control points that extremize the action. They are tabulated in Table 1, and the function $\varpi_1(\psi)$ is interpolated between these points as described in the previous

section.

$\bar{\beta}$	$\varpi_1(0.0)$	$\varpi_1(0.2)$	$\varpi_1(0.4)$	$\varpi_1(0.6)$	$\varpi_1(0.8)$	$\varpi_1(0.99)$
1.0	29.687	29.817	23.281	18.809	8.310	6.000
2.0	28.281	29.165	24.644	17.774	11.150	6.000
3.0	28.384	28.985	23.990	19.965	10.139	6.000

Table 1: Values of control points $\varpi_1(\psi_i)$ that yield a local extremum of the action. The last value $\varpi_1(0.99)$ is fixed as a boundary condition.

For each converged solution, we can numerically integrate the asymptotic equation to evaluate $I(\psi)$. For practical purposes, we present here an interpolation formula that is a seventh degree polynomial in β^{-1}, and the coefficients are tabulated in Table 2. Once $I(\psi)$ is known, one may determine the outer boundary of the computational domain in accordance with the asymptotic condition (4-10). With the combination of $\varpi_1(\psi)$ and $I(\psi)$, we are able to reconstruct the streamlines with the spline interpolation scheme, and they are depicted in Figure 3. The location of the Alfvén surface determines the value of J as a function of ψ, which ultimately allows us to compute the angular momentum being transported as well as the terminal velocity along each streamline. For convenience, we also present an interpolation formula for $J(\psi)$ as a polynomial in β, with the coefficients tabulated in Table 3.

$\bar{\beta}$	I_0	I_1	I_2	I_3	I_4	I_5	I_6	I_7
1	0.732	-0.446	0.886	-0.511	-1.781	2.648	-1.397	0.263
2	0.842	0.413	-2.504	2.699	-11.768	24.849	-22.870	7.602
3	1.164	-2.915	30.674	-194.996	585.524	-998.495	930.236	−347.764

Table 2: Interpolation formula for $I_{\rm int}(\psi) = \sum_{i=0}^{7} I_i \beta^{-i}$. The interpolated function agrees with the numerical values to within 0.5%.

$\bar{\beta}$	J_0	J_1	J_2	J_3	J_4	J_5	J_6	J_7	$\bar{J}$
1	-2.791	17.214	-13.640	-10.294	22.483	-13.656	3.628	-0.362	2.638
2	-14.944	45.162	-43.065	21.660	-6.265	1.057	-0.0969	0.00373	4.356
3	-20.285	40.676	-25.088	8.006	-1.440	0.148	-0.00825	0.000191	6.202

Table 3: Interpolation formula for $J_{\rm int}(\psi) = \sum_{i=0}^{7} J_i \beta^{i}$. The last column gives the value $\bar{J}$ of $J(\psi)$ averaged over ψ from 0 to 0.99. The interpolated function agrees with the numerical values to within 1%.

The solid lines in Figure 3 show the logarithmically spaced contours of constant density. It is evident that even though the dotted streamlines become asymptotically

radial and only collimate logarithmically slowly, the density becomes cylindrically stratified very quickly, giving the X-wind the illusion of a jet-like appearance (Shang et al. 1998, 2002).

Detailed comparisons of the results obtained here with those given by Shang (1998) show some differences, but the main impression is how remarkably well the solutions obtained by the two very different methods for the same mass-to-flux loading $\beta(\psi)$ agree with one another. Shang (1998) had a similar experience in comparing her approximate, but analytic, solutions for the sub-Alfvénic region to the exact, but numerical, solutions obtained by Najita & Shu (1994).

We attribute the fortunate circumstance to the following causes. If one is given somehow the geometric shape of the streamlines (or, equivalently, the field lines in the meridional plane), then the Weber-Davis procedure used by Shang, which includes an exact solution of Bernoulli's equation, would give an exact solution of the two-dimensional flow problem, provided one takes care to cross each of the critical points properly. In realistic circumstances, the geometric shape of streamlines in the meridional plane is not given a priori, but is to be found from the Grad-Shafranov equation (or, equivalently, from minimizing the action by variations of the stream function ψ). However, if one has analytic solutions to the Grad-Shafranov equation (from the work of Shu et al. 1994b and 1995) near and far from the X-point, then there are only so many ways that one can adjust the function $z(\varpi, \psi)$ for values of ψ from 0 to 1 and of ϖ close to 1 (or dimensionally, R_X) to $\varpi \gg 1$ (or R_X) that will connect the shape of the streamlines near the X-point (a fan) smoothly to those appropriate at asymptotic infinity (radial outflow). The procedures used by Shang (1998) and those used here to make such adjustments differ, but the global solution is relatively insensitive to these details as long as one gets the conserved quantities: mass-to-flux loading $\beta(\psi)$, angular momentum distribution $J(\psi)$, and Bernoulli's constant $H(\psi) = 0$ correctly.

7. Discussion and Conclusions

7.1. Recipe for Use of Results

For the convenience of the reader, we summarize the recipes needed to convert the results of the previous section into numerical X-wind models for astronomical and meteoritical applications. Begin with the equation that describes the dimensionless locus of a streamline for given ψ with numerical value between 0 and 1:

$$z = z(\varpi, \psi), \tag{7-1}$$

where the functional form of $z(\varpi, \psi)$ is computed numerically by the technique described in §5.2.

The reconstruction of streamline shapes, i.e., the function $z(\varpi, \psi)$, is performed over three radial intervals whose end points are $\varpi_0 \equiv 1$, $\varpi_1(\psi) > 1$, $\varpi_2(\psi) > \varpi_1(\psi)$, and $\varpi_3(\psi) \equiv \varpi_\infty(\psi) > \varpi_2(\psi)$ that give a geometrically increasing separation:

$$\frac{\varpi_2 - \varpi_1}{\varpi_1 - 1} = \frac{\varpi_\infty - \varpi_2}{\varpi_2 - \varpi_1}, \tag{7-2}$$

where $\varpi_\infty(\psi)$ is given by equation (5-7):

$$\varpi_\infty = \frac{2\bar{\beta}}{C} \frac{\cosh[C^{-1} I(C, 1)]}{\cosh[C^{-1} I(C, \psi)]}. \tag{7-3}$$

For practical computations, we choose $C = 0.1\bar{\beta}$ so that $\varpi_\infty = 20$ on the $\psi = 1$ streamline. The asymptotic integral $I(C, \psi)$ in equation (4-10) can be approximated by a seventh degree polynomial in β^{-1}:

$$I(\psi) = I_0 + I_1 \beta^{-1}(\psi) + \ldots + I_7 \beta^{-7}(\psi), \tag{7-4}$$

where the coefficients I_0, I_1, ..., I_7 are given in Table 2 for the three values of $\bar{\beta} = 1, 2, 3$. The function $\varpi_1(\psi)$ represents the first nontrivial abscissa of the spline beyond the X-point for each value of ψ and is tabulated in Table 1 for $\psi_i = 0.0, 0.2, 0.4, 0.6, 0.8, 0.99$. For intermediate values, we interpolate ϖ_1 by a piecewise cubic polynomial:

$$\varpi_1 = h_0(\psi_i) + h_1(\psi)(\psi - \psi_i) + h_2(\psi_i)(\psi - \psi_i)^2 + h_3(\psi_i)(\psi - \psi_i)^3 \text{for} \psi_\text{i} \leq \psi < \psi_{\text{i+1}}. \tag{7-5}$$

In Table 4, we list the values of $h_j(\psi_i)$ for each case of $\bar{\beta}$. To get $\varpi_2(\psi)$ for any value of ψ, one should use equation (7-2) after first computing $\varpi_1(\psi)$ and $\varpi_\infty(\psi)$ at the desired value of ψ.

The shape of each streamline given by $\psi = \text{const}$ in the three radial intervals whose end points are $\varpi_0(\psi) = 1$, $\varpi_1(\psi)$, $\varpi_2(\psi)$, and $\varpi_3(\psi) = \varpi_\infty(\psi)$ is then described by a piecewise cubic polynomial, whose form, suppressing the implicit dependence on ψ, is given by equation (5-11):

$$z(\varpi) = y_1 a + y_2 b + \frac{(\varpi_{i+1} - \varpi_i)^2}{6} \left[f_1(a^3 - a) + f_2(b^3 - b) \right], \tag{7-6}$$

where

$$a \equiv \frac{\varpi_{i+1} - \varpi}{\varpi_{i+1} - \varpi_i}, \qquad b \equiv \frac{\varpi - \varpi_i}{\varpi_{i+1} - \varpi_i}. \tag{7-7}$$

The coefficients y_1, y_2, f_1, and f_2 are listed in Table 5 for discrete values of $\psi = 0.0$, 0.2., 0.4, 0.6, 0.8, 0.99 in the three cases $\bar{\beta} = 1, 2, 3$. A Hyman limited spline may be used to compute the streamlines for other values of ψ.

The partial derivatives of ψ with ϖ or z are now given by the usual rules of multivariate calculus:

$$\left(\frac{\partial \psi}{\partial \varpi} \right)_z = -\frac{(\partial z / \partial \varpi)_\psi}{(\partial z / \partial \psi)_\varpi}; \qquad \left(\frac{\partial \psi}{\partial z} \right)_\varpi = \frac{1}{(\partial z / \partial \psi)_\varpi}. \tag{7-8}$$

	ψ	0.0	0.2	0.4	0.6	0.8
$\bar{\beta}=1$	h_0	29.687	29.817	23.281	18.809	8.310
	h_1	17.315	−1.950	−27.520	−37.428	−31.809
	h_2	−153.650	−333.100	126.938	−254.103	103.428
	h_3	351.625	897.250	−505.688	893.830	0.000
$\bar{\beta}=2$	h_0	28.281	29.165	24.644	17.774	11.150
	h_1	17.933	−9.093	−28.478	−33.735	−30.035
	h_2	−67.563	−105.763	−61.800	−9.272	15.422
	h_3	0.000	191.000	162.188	61.737	0.000
$\bar{\beta}=1$	h_0	28.384	28.985	23.990	19.965	10.139
	h_1	16.995	−9.015	−22.550	−34.628	−35.107
	h_2	−79.800	−171.725	96.763	−215.142	70.117
	h_3	49.250	459.625	−423.188	713.150	0.000

Table 4: Interpolation coefficients for $\varpi_1(\psi)$

Table 3 gives $J(\psi)$ as a seventh order polynomial in $\beta(\psi)$:

$$J(\psi) = J_0 + J_1\beta(\psi) + \ldots + J_7\beta^7(\psi), \tag{7-9}$$

where $\beta(\psi)$ is itself given by

$$\beta(\psi) = \frac{2}{3}\bar{\beta}(1-\psi)^{-1/3}, \tag{7-10}$$

with $\bar{\beta} = 1$, 2, 3 in the three chosen model cases. The coefficients tabulated in Table 3 give a $J(\psi)$ that guarantees that equation (2-13b),

$$|\nabla\psi|^2 + \frac{1}{\mathcal{A}^2}\left(\frac{J}{\varpi^2} - 1\right)^2 + \frac{2\varpi^2 V_{\text{eff}}}{(\beta^2 - \varpi^2\mathcal{A})^2} = 0, \tag{7-11}$$

has one real root for $\mathcal{A}$ in the computational domain when V_{eff} is given by equation (2-2):

$$V_{\text{eff}} = -\frac{1}{\sqrt{\varpi^2 + z^2}} - \frac{1}{2}\varpi^2 + \frac{3}{2}. \tag{7-12}$$

By solving equation (7-11) as a fourth-order polynomial, we may obtain the relevant value for the Alfvén discriminant $\mathcal{A}$. Then the density can be computed through equation (2-9)

$$\rho = (\beta^2 - \varpi^2\mathcal{A})^{-1}. \tag{7-13}$$

Note that this equation produces $\rho = \beta^{-2}$ at the Alfvénic transition $\mathcal{A} = 0$.

With the density in place, we may obtain the two components of dimensionless poloidal velocity from the definition (2-3) of ψ:

$$u_\varpi \equiv \frac{1}{\varpi\rho}\frac{\partial\psi}{\partial z}, \quad u_z \equiv -\frac{1}{\varpi\rho}\frac{\partial\psi}{\partial\varpi}. \tag{7-14}$$

	ψ	0.0	0.2	0.4	0.6	0.8	0.99
$\bar{\beta}=1$	y_1	0.0	12.764	21.872	41.255	51.367	525.487
	y_2	0.0	366.579	627.01	1044.15	1402.6	3648.96
	f_1	0.0	3.834×10^{-3}	3.083×10^{-2}	0.256	4.120	118.485
	f_2	0.0	-2.901×10^{-5}	-4.685×10^{-4}	-1.033×10^{-2}	−0.301	−48.051
$\bar{\beta}=2$	y_1	0.0	12.091	22.694	29.659	37.935	73.230
	y_2	0.0	86.922	156.801	208.943	267.766	383.996
	f_1	0.0	2.359×10^{-3}	1.489×10^{-2}	9.705×10^{-2}	0.750	9.943
	f_2	0.0	-1.991×10^{-4}	-1.518×10^{-3}	-1.333×10^{-2}	−0.158	−4.246
$\bar{\beta}=3$	y_1	0.0	14.138	22.415	33.841	26.286	44.094
	y_2	0.0	82.541	104.01	133.299	131.469	173.659
	f_1	0.0	1.903×10^{-2}	2.353×10^{-2}	5.056×10^{-2}	0.376	2.950
	f_2	0.0	-3.651×10^{-3}	-5.610×10^{-3}	-1.722×10^{-2}	−0.102	−1.424

Table 5: Spline coefficients for the streamlines.

The toroidal velocity in the corotating frame is given by equation (2-6)

$$u_\varphi = \frac{J(\psi)-\varpi^2}{\varpi(1-\beta^2\rho)}. \tag{7-15}$$

Note that $J(\psi)=\varpi^2$ where $\beta^2\rho=1$ keeps the toroidal velocity u_φ well-behaved across the Alfvén surface, which is not one of the critical surfaces of the overall problem.

The vector magnetic field may now be obtained from equation (2-4):

$$\mathbf{B} = \beta\rho\mathbf{u}, \tag{7-16}$$

whereas the azimuthal velocity in the inertial frame is given by

$$v_\varphi = u_\varphi + \varpi, \tag{7-17}$$

with the term ϖ from the frame rotation being cancelled at large ϖ where $u_\varphi \to -\varpi$ because ρ vanishes as $1/\varpi^2$ at large distances from the rotation axis. Finally, to convert the computed quantities to their dimensional counterparts, we must multiply velocities, densities, and magnetic fields by $R_X\Omega_X$, $\dot{M}_w/4\pi R_X^3\Omega_X$, and $(\Omega_X\dot{M}_w/R_X)^{1/2}$, respectively.

For interpolations or extrapolations in $\bar{\beta}$, we recommend computation first of the dimensionless density, velocity, and magnetic fields for the three cases $\bar{\beta}=1$, 2, 3, and then direct interpolations or extrapolations of those fields. Other techniques starting farther back in the process run the danger of obtaining complex roots of $\mathcal{A}$ (i.e., complex values of ρ) from the solution of the quartic equation (7-11) because of slight inaccuracies in computing the numerical coefficients.

7.2. Summary

In this paper, we have presented a technique by which solutions to the so-called Grad-Shafranov equation for X-wind flow can be solved, not by attacking the partial differential equation directly, but by choosing trial functions that minimize an appropriate action integral. While this method has been applied before in problems of plasma confinement in the fusion community, we believe that the example given here is its first application in astrophysics for the notorious case when magnetohydrodynamical flows cross critical surfaces that change the character of the underlying PDE.

Many empirical arguments suggest that funnel flows and X-winds do underlie the accretion hot-spots, jets, and winds of YSOs, although a dipolar field geometry near the star (see Fig. 1) may be an over-simplification (Ardila et al. 2002, Unruh et al. 2004, Johns-Krull 2007). Fortunately, although the fractional areal coverage of hot spots depends on the detailed multipole structure of the surfaces of actual young stars, the general validity of X-wind theory depends only on the level of trapped flux in the X-region and is insensitive to the magnetic geometry on the star as long as the fields are strong (Mohanty & Shu 2007). The trapped flux in the X-wind models of this paper are computed as

$$2\pi\bar{\beta}\left(\frac{GM_*\dot{M}_w}{\Omega_X}\right)^{1/2}, \tag{7-18}$$

and should be compared with the magnetic flux (area times mean field) in hot-spots on one hemisphere's surface of the star impacted by the corresponding funnel flow. (Both fluxes are 1/3 of the total trapped flux in the X-region and equal the net flux of the dead region.) For T Tauri stars, the comparison is pretty good (see, e.g., Johns-Krull & Gafford 2002).

Apart from relative simplicity, the semi-analytical solutions summarized in §7.1 have many other advantages. For example, the solutions hold over a formally infinite dynamic range, showing the asymptotic, logarithmically slow, collimation into jets missing in many numerical simulations. These properties make the models of this paper especially suitable for a wide variety of astronomical and meteoritical applications, such as detailed comparisons with observations, trajectories of solids entrained in the wind, and interactions with neighboring circumstellar or interstellar matter. A needed generalization for future research is the inclusion of the effects of the intrinsic magnetization of the surrounding accretion disk.

We thank the Physics Department and the Center for Astrophysics and Space Sciences of UCSD for support. The Academia Sinica and the National Science Council (NSC) of Taiwan also provided funding through their grants to the Theoretical

Institute for Advanced Research in Astrophysics (TIARA). The research of MJC is supported in part by the NSC grant 95-2112-M-001-44.

A. Character of Governing Equation

The GSE (2-7) resembles the steady state heat diffusion equation with a variable diffusion coefficient $\mathcal{A}$. This analogy is actually misleading since we do not know its overall character until we substitute in the implicit dependence of $\mathcal{A}$ on ψ by solving the (algebraic) BE and examine the characteristics of the GSE. To do so, let us first differentiate the BE with respect to ϖ and z.

$$\begin{aligned}
&2(\psi_{,\varpi}\psi_{,\varpi\varpi}+\psi_{,z}\psi_{,z\varpi})-\frac{2\mathcal{A}_{,\varpi}}{\mathcal{A}^3}\left(\frac{J}{\varpi^2}-1\right)^2\\
&\qquad+\frac{2\varpi^4\mathcal{A}_{,\varpi}}{(\beta^2-\varpi^2\mathcal{A})^3}\left[2V_{\rm eff}+2\epsilon^2\ln\left(\frac{\epsilon^2 h}{\beta^2-\varpi^2\mathcal{A}}\right)+\epsilon^2\right]+...=0,\\
&2(\psi_{,\varpi}\psi_{,\varpi z}+\psi_{,z}\psi_{,zz})-\frac{2\mathcal{A}_{,z}}{\mathcal{A}^3}\left(\frac{J}{\varpi^2}-1\right)^2\\
&\qquad+\frac{2\varpi^4\mathcal{A}_{,z}}{(\beta^2-\varpi^2\mathcal{A})^3}\left[2V_{\rm eff}+2\epsilon^2\ln\left(\frac{\epsilon^2 h}{\beta^2-\varpi^2\mathcal{A}}\right)+\epsilon^2\right]+...=0,
\end{aligned}$$

where in the above equations, a subscript denotes partial derivative and the ellipsis symbols include terms that are irrelevant in determining the character of the GSE. These equations may be solved for $\mathcal{A}_{,\varpi}$ and $\mathcal{A}_{,z}$ to give

$$\mathcal{A}_{,\varpi}=\frac{1}{\mathcal{P}}(\psi_{,\varpi}\psi_{,\varpi\varpi}+\psi_{,z}\psi_{,z\varpi})+...,\qquad \mathcal{A}_{,z}=\frac{1}{\mathcal{P}}(\psi_{,\varpi}\psi_{,\varpi z}+\psi_{,z}\psi_{,zz})+...,$$

where

$$\mathcal{P}=\frac{\varpi^2}{\beta^2-\varpi^2\mathcal{A}}|\nabla\psi|^2+\frac{1}{\mathcal{A}^3}\left(\frac{J}{\varpi^2}-1\right)^2\frac{\beta^2}{\beta^2-\varpi^2\mathcal{A}}-\frac{\epsilon^2\varpi^4}{(\beta^2-\varpi^2\mathcal{A})^3},$$

after we eliminate $V_{\rm eff}$ in the expression by using the BE (2-13b). The second derivative terms in the GSE (2-13a) can now be written in the form

$$a\psi_{,\varpi\varpi}+2b\psi_{,\varpi z}+c\psi_{,zz}+...=0,$$

where

$$a=\mathcal{A}+\frac{\psi_{,\varpi}^2}{\mathcal{P}},\qquad b=\frac{\psi_{,\varpi}\psi_{,z}}{\mathcal{P}},\qquad c=\mathcal{A}+\frac{\psi_{,z}^2}{\mathcal{P}}.$$

The character of the GSE is determined by the quantity $\Delta=b^2-ac$ (Garabedian 1986): it is elliptic, parabolic, or hyperbolic if Δ is negative, zero, or positive. We may compute Δ for our GSE explicitly.

$$\Delta=-\mathcal{A}^2\left\{\frac{|\nabla\psi|^2+(J\varpi^{-2}-1)^2\mathcal{A}^{-2}-\epsilon^2\mathcal{A}\varpi^4[\beta(\beta^2-\varpi^2\mathcal{A})]^{-2}}{\varpi^2\mathcal{A}\beta^{-2}|\nabla\psi|^2+(J\varpi^{-2}-1)^2\mathcal{A}^{-2}-\epsilon^2\mathcal{A}\varpi^4[\beta(\beta^2-\varpi^2\mathcal{A})]^{-2}}\right\}. \quad \text{(A1)}$$

The interpretation of this expression becomes transparent if we transform back into the physical quantities. After some algebra, we have

$$\Delta = -\mathcal{A}^2\left[\frac{u^2-\epsilon^2(1-M_A^2)}{(1-M_A^2)(u_p^2-\epsilon^2)+u_\varphi^2}\right] = \mathcal{A}^2\left[\frac{(v_A^2+\epsilon^2)(u_p^2-v_s^2)}{(u_p^2-v_{-p}^2)(u_p^2-v_{+p}^2)}\right]. \tag{A2}$$

where $v_{Ap} \equiv \sqrt{B_p^2/\rho}$ is the poloidal component of the Alfvén velocity $v_A \equiv \sqrt{B^2/\rho}$ with $B^2 = B_p^2 + B_\varphi^2$, u_p is the poloidal fluid velocity, and v_s is defined by

$$v_s^2 \equiv \frac{\epsilon^2 v_{Ap}^2}{v_A^2+\epsilon^2}.$$

In the limit where $v_A^2 \gg \epsilon^2$, it reduces to the thermal sound speed. In addition, $v_{\pm p}$ denote the poloidal component of the fast and slow MHD wave speeds, respective, and are given by

$$v_{\pm p}^2 = \frac{1}{2}(v_A^2+\epsilon^2)\left[1 \pm \sqrt{1-\frac{4v_s^2}{v_A^2+\epsilon^2}}\right]. \tag{A3}$$

A moment of thought reveals that $v_s < v_{-p} < v_{+p}$. The significance of the equation (A2) is now clear. The governing GSE is elliptic when $u_p^2 < v_s^2$ or $v_{-p}^2 < u_p^2 < v_{+p}^2$, and it is hyperbolic when $v_s^2 < u_p^2 < v_{-p}^2$ or $u_p^2 > v_{+p}^2$ (19; 39).

To be definite, we shall refer to the loci where the poloidal velocity squared equals v_s^2, v_{-p}^2 and v_{+p}^2 as sonic, slow, and fast surfaces, respectively. Despite the deceiving appearance of the GSE (2-7), note that it does not change character on the Alfvén surface when $\mathcal{A} = 0$ (or equivalently when $M_A = 1$ and the total fluid velocity in the corotating frame equals the total Alfvén speed); it remains elliptic until the fast surface. The fact that the asymptotic flow is described by a hyperbolic PDE is consistent with our physical intuition. When the fluid speed is super-magnetosonic, no information can be sent upstream into the flow. Thus the asymptotic behavior of the X-wind is determined by the "initial condition" at the place when the fluid velocity first becomes equal to the fastest signal propagation speed – a defining feature of hyperbolic problems.

In the cold limit the discriminant Δ has the simplification,

$$\Delta = -\mathcal{A}^2\left\{\frac{|\nabla\psi|^2 + (J\varpi^{-2}-1)^2\mathcal{A}^{-2}}{\varpi^2\mathcal{A}\beta^{-2}|\nabla\psi|^2 + (J\varpi^{-2}-1)^2\mathcal{A}^{-2}}\right\} = -\mathcal{A}^2\left(\frac{1}{1-u_p^2/v_A^2}\right). \tag{A4}$$

This equation explicitly states that the transition to the hyperbolic portion of the solution is done through the fast surface, where the poloidal fluid velocity is equal to the magnetosonic speed, which is the total Alfvén speed $v_A = B/\sqrt{\rho}$ when ϵ is set to zero. The axial symmetry of the assumed problem guarantees that any compressions or rarefactions occur only in the meridional plane, so the relevant speed of signal propagation in the limit $\epsilon \to 0$ is the magnetosonic speed relative to the poloidal motion of the fluid.

REFERENCES

Ardila, D. R., Basri, G., Walter, F. M., Valenti, J. A., Johns-Krull, C. M. 2002, ApJ, 567, 1013

Askey, R. 1982 Lett. in Math. Phys, 6, 299

Bacciotti, F., Ray, T. P., Eislöffel, J., Solf, J. 2002, ApJ, 576, 222

Blandford, R. D., Rees, M. J. 1992, in Testing the AGN Paradigm, AIP Conf. Proc., 254, 3

Blandford, R. D., Payne, D. G. 1982 MNRAS, 199, 883

Bouvier, J. 1990, AJ, 99, 946

Cabrit, S., Pety. J., Presenti, N., Dougados, C. 2006, A&A, 452, 897

Camenzind, M. 1987, A&A, 184, 341

Coffey, D., Bacciotti, F., Woitas, J., Ray, T. P., Eislöffel, J. 2004, ApJ, 604, 708

Coffey, D., Bacciotti, F., Ray, T. P., Esilöffel, J., Woitas, J. 2007, ApJ, 663, 350

Contopoulos, J., Lovelace, R.V.E. 1994, ApJ, 429, 139

Edwards, S., Ray, T., Mundt, R. 1993, in Protostars & Planets III, ed. E. H. Levy & J. Lunine (Tucson: Univ. of Arizona Press), 567

Ferreira, J. 2004, Ap&SS, 293, 83

Garabedian, P. R. 1986, Partial Differential Equations, (Providence: Americal Mathematical Society)

Giampapa, M.S., Basri, G., Johns, C.M., Imhoff, C.L. 1993, ApJS, 89, 321

Goldreich, P., Julian, W. H. 1970, ApJ, 160, 971

Goodson, A. P., Bohm, K. H., Winglee, R. M. 1999, ApJ, 524, 142

Grad, H., Rubin, H. 1958, in Proc. Conf. Internat. Atomic Energy Agency 31, (Geneva: Internat. Atomic Energy Agency)

Heinemann, M., Olbert, S. 1978, JGR, 83, 2457

Heyvaerts, J., Norman, C.A. 1997, in Herbig–Haro Flows and the Birth of Stars, IAU Symp. 182, ed. B. Reipurth & C. Bertout (Kluwer), 275

Hyman, J. 1983, SIAM, J. Sci. Stat. Comput., 4, 645

Jackson, J. D. 1975, Classical Electrodynamics, (New York: John Wiley & Sons)

Johns, C., Basri, G. 1995, ApJ, 449. 341

Johns-Krull, C. M. 2007, arXiv0704.2923v1 [astro-ph]

Johns-Krull, C. M., Gafford, A. D. 2002, ApJ, 573, 685

Johns-Krull, C.M., Hatzes, A.P. 1997, ApJ, 487, 896

Königl, A., Pudritz, R. E. 2000, in Protostars & Planets IV, ed. V. Mannings, A. P. Boss, & S. S. Russell (Tucson: Univ. of Arizona Press), 759

Long, M., Romanova, M. M., Lovelace, R. V. E. 2005, ApJ, 634, 1214

Lovelace, R.V.E., Mehanian, C., Mobarry, C.M., Sulkanen, M.E. 1986, ApJS, 62, 1

Mestel, L. 1968, MNRAS, 138, 359

Mohanty, S., Shu, F.H. 2007, ApJ, in preparation

Najita, J. R., Carr, J. S., Glassgold, A. E., Valenti. J. A. 2007, Protostars & Planets V, ed. B. Reipurth, D. Jewitt, & K. Keil (Tucson: Univ. of Arizona Press), 507

Najita, J. R., Shu, F. H. 1994, ApJ, 429, 808

Ostriker, E. C., Shu, F. H. 1995, ApJ, 447, 813

Pety, J., Gueth, F., Guilloteau, S., Dutrey, A. 2006, A&A, 458, 841

Press, W. H., Teukolsky, S. A., Vetterling, W. T., & Flannery, B. P. 1992, Numerical Recipes in C++ (Cambridge University Press)

Pudritz, R.E., Rogers, C.S., Ouyed, R. 2006, MNRAS, 365, 113

Ramsay, J. O. 1988, Statist. Sci., 3, 425

Ramsay, J. O. 1998, J. R. Statist. Soc. B, 60, Part 2, 365

Sakurai, T. 1985, A & A, 152, 121

Shafranov, V. D. 1966, Rev. Plasma Phys, 2, 103

Shang, H. 1998, PhD Thesis, Univ. of California, Berkeley

Shang, H., Shu, F. H., Glassgold, A. E. 1998, ApJ, 493, 91

Shang, H., Glassgold, A. E., Shu, F. H., Lizano, S. 2002, ApJ, 564, 853

Shang, H., Lizano, S., Glassgold, A. E., Shu, F. H. 2004, ApJ, 612, L69

Shu, F. H., Lizano, S., Ruden, S. P., Najita, J. 1988, ApJ, 328, L19

Shu, F. H. 1992, The Physics of Astrophysics, Vol II: Gas Dynamics, (Mill Valley: University Science Books)

Shu, F. H., Najita, J., Ostriker, E., Wilkin, F., Ruden, S., Lizano, S. 1994 ApJ, 429, 781

Shu, F. H., Najita, J., Ruden, S. P., Lizano, S. 1994b, ApJ, 429, 797

Shu, F. H., Najita, J., Ostriker, E. C., Shang, H. 1995 ApJ, 455, L155

Shu, F. H., Najita, J. R., Shang, H., Li, Z.-Y., 2000, in Protostars & Planets IV, ed. V. Mannings, A. P. Boss, & S. S. Russell (Tucson: Univ. of Arizona Press), 789

Shu, F. H., Shang, H., Gounelle, M., Glassgold, A. E., Lee, T. 2001, ApJ, 548, 1029

Tsinganos, K., Trussoni, E. 1991, A&A, 249, 156

Uchida, Y., Shibata, K. 1985, PASJ, 37, 515

Unruh, Y. C. et al. 2004, MNRAS, 348, 1301

Ustyugova, G.V., Koldoba, A., Romanova, M.M., Lovelace, R.V.E. 2006, 646, 304

Van Dyke, M. 1964 Perturbation Methods in Fluid Mechanics, (New York: Academic Press)

Vogel. S., Kuhi, L. 1981, ApJ, 245, 960

Weber, E. J., Davis, L. 1967, ApJ, 148, 217

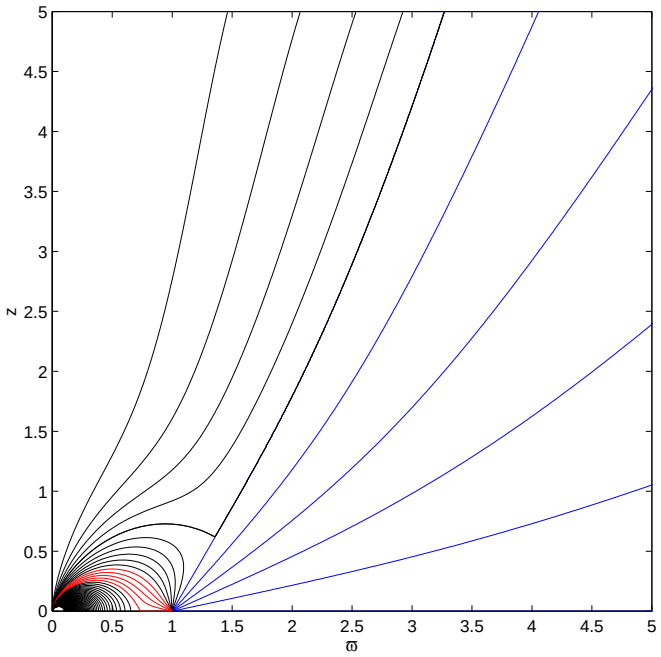

Fig. 1.— Funnel flow (red curves), X-wind streamlines (blue curves), and field lines dead to magnetocentrifugal fling (black curves) according to Ostriker & Shu (1995) and Shang et al. (1998). The magnetic field near the origin (center of YSO) is modeled as a magnetic dipole, and all of the field lines contained in the X-wind have their counterparts (with reversed directions) in opened stellar field lines that lie inside a hollow cone dead to flow surrounding the z-axis. Exact pressure balance across the sheet current that divides the X-wind and dead field lines holds near and far from the Y-point at $\varpi \approx 1.3$, $z \approx 0.7$, but this balance is only approximate at intermediate distances, which accounts for why the tilted upside-down Y of the separatrix does not have the equal angles of 120° that would characterize an exact Y-configuration appropriate for coronal conditions. In fact, the field lines in red and black are computed as if they were vacuum magnetic fields; only the portion depected in blue are attacked via the solution of the Grad-Shafranov equation or its variational-principle analog discussed in the present paper. The neutral line separating the black and blue field lines is replaced by a separatrix of prescribed locus satisfying the approximate pressure balance as described above. (see §4).
The implied poloidal and toroidal current flows are discussed in Ostriker & Shu (1995) and Shu et al. (1995); in particular, there is no current flow along the z-axis which is taken to be a region of vacuum longitudinal field.

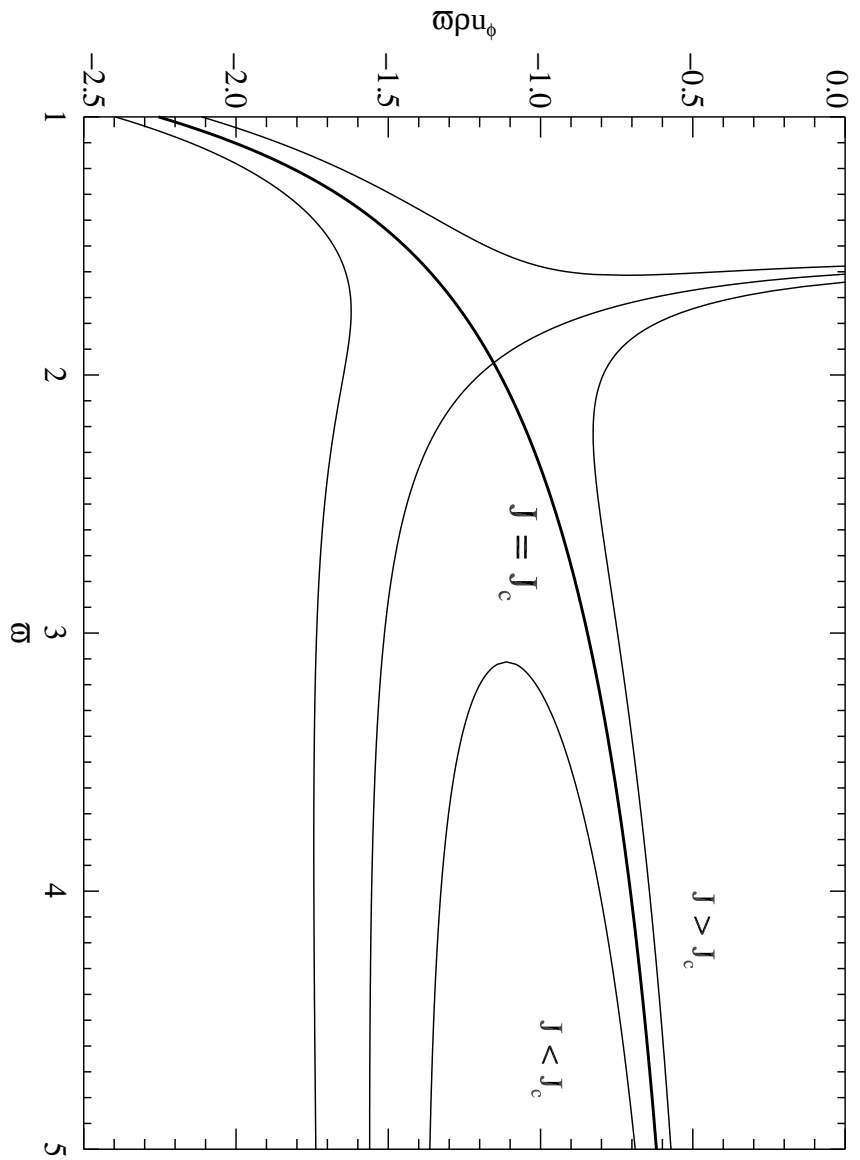

Fig. 2.— Determination of the critical value of J that allows a fast mode transition

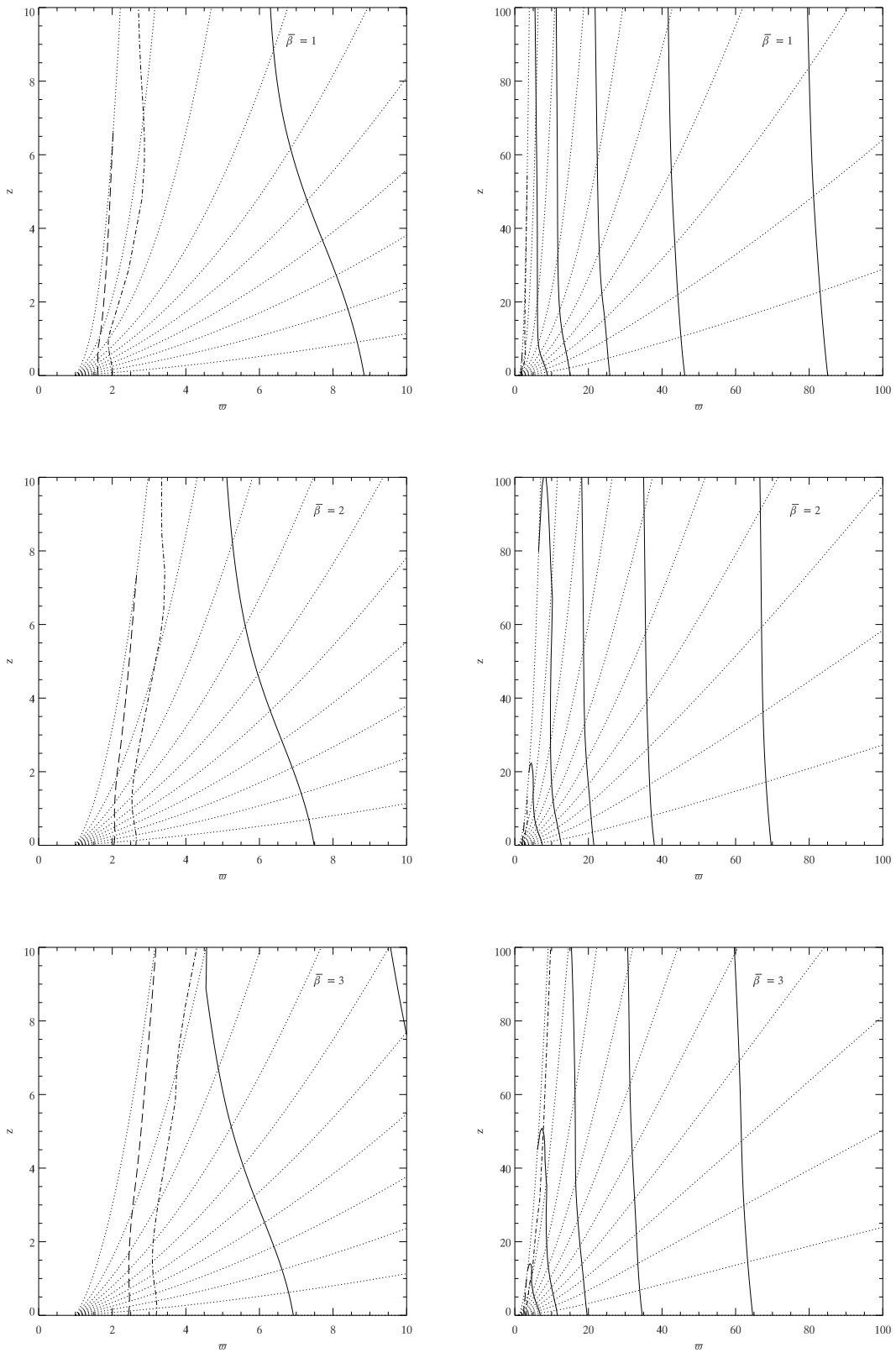

Fig. 3.— Solutions for $\bar{\beta} = 1, 2, 3$. The dotted curves represent the streamlines labeled by constant ψ, and the solid curves are isodensity contours separated by